CrystEngComm

Accepted Manuscript

ROYAL SOCIETY OF CHEMISTRY

www.rsc.org/crystengcomm

Journal Name

ARTICLE

Establishing Template-induced Polymorphic Domains for API Crystallisation: The case of Carbamazepine

Received 00th January 20xx,
Accepted 00th January 20xx

DOI: 10.1039/x0xx00000x

www.rsc.org/

Jose V. Parambil,[a,b] Sendhil K. Poornachary,[c] Steve J. Hinder,[d] Reginald B. H. Tan*[,b,c] and Jerry Y. Y. Heng*[,a]

Template-induced nucleation of the model compound, Carbamazepine (CBZ), on substrates with different surface chemistries was studied. Supersolubility regions in which CBZ metastable form II or stable form III preferentially nucleated under the influence of cyano-, mercapto- and fluoro-functionalised templates were determined. Analysis of the resulting Template-induced Polymorphic Domain (TiPoD) plots indicated that cyano-functionalised templates promoted nucleation of form II and, in contrast, mercapto and fluoro surfaces favoured nucleation of form III. By comparing the interaction energies between CBZ crystal polymorphs and each template surface using molecular simulations, we propose that intermolecular interactions during the early stages of crystal nucleation selectively favours heterogeneous nucleation and growth of specific polymorphs on the functionalised surfaces. In the light of recent studies relating solvent effects to preferential nucleation of CBZ polymorphs, we further discuss the role of surface chemistry in directing the molecular-assembling process en route template-induced crystal nucleation.

Introduction

Polymorphism is a significant aspect of crystallisation of organic small molecules, especially in the pharmaceutical sector. Apart from the thermodynamic free energy differences between crystal polymorphs which affects the dissolution rates and equilibrium solubility of active pharmaceutical ingredients (APIs), differences in bulk crystal properties can also influence secondary processing characteristics such as the ease of filtration, compressibility and flowability.[1,2] Appearance of polymorphs during solution crystallisation is governed by both thermodynamic and kinetic aspects of nucleation and growth. As a result, a plethora of crystallisation methods have been developed to discover the thermodynamically stable as well as kinetically favoured polymorphic forms. Some of the common methods to generate supersaturation involve cooling, evaporation, and antisolvent addition.[3] Even under these broad realm of methods, the rate of supersaturation generation can be varied significantly thereby affecting the nucleation kinetics of different polymorphs.[4] The process of seeding is frequently used in pharmaceutical crystallisation to achieve polymorph selectivity.[3] This involves adding small quantities of seed crystals of the desired polymorphic form to the supersaturated solution, thus enabling crystal growth and promoting secondary nucleation. However, inconsistencies in the seed crystal properties[5] and cross-nucleation between crystal polymorphs[6,7] can result in unwanted crystal polymorphs and thereby affect product quality. Additionally, unintentional dust particles in solution and the vessel surfaces may also induce crystal nucleation heterogeneously, posing significant challenges to polymorph control.

Homogeneous crystal nucleation is energetically more demanding than heterogeneous nucleation due to the energy penalty associated with the creation of a crystal–solution interface.[8] On the other hand, template-induced nucleation can provide a favourable heterogeneous nucleation pathway for crystallisation. In this case, the crystal nucleus attaches to the template surface and thereby decreases the activation energy barrier by reducing the interfacial area between the nucleus and solution. In general, the effect of templates on heterogeneous nucleation can be expected to be dominant near the concomitant nucleation region wherein the thermodynamic, structural, and kinetic factors influencing the nucleation rates of different polymorphs are in delicate balance with each other. Templates can be well-ordered two[9] or three dimensional[10] structures such as organic and inorganic crystal surfaces,[11,12] self-assembled monolayers[13, 14] or colloidal particles.[15,16] Likewise, amorphous structures such as polymers[17,18] and gels[19] have been used in template-assisted nucleation. Besides epitaxial relationship between the

[a] Surfaces and Particle Engineering Laboratory, Department of Chemical Engineering, Imperial College London, South Kensington Campus, London SW7 2AZ, United Kingdom.
[b] Department of Chemical and Biomolecular Engineering, National University of Singapore, 4 Engineering Drive 4, Singapore 117585.
[c] Institute of Chemical and Engineering Sciences, A*STAR (Agency for Science, Technology and Research), 1 Pesek Road, Jurong Island, Singapore 627833
[d] The Surface Analysis Laboratory, Faculty of Engineering & Physical Sciences, University of Surrey, Guildford, Surrey GU2 7XH, United Kingdom
Electronic Supplementary Information (ESI) available: [includes XPS, contact angle analysis and ellipsometry on template surfaces]. See DOI: 10.1039/x0xx00000x
*(R.B.H.T) – reginald_tan@ices.a-star.edu.sg
*(J.Y.Y.H) – jerry.heng@imperial.ac.uk

template substrate and the nucleating crystal structure, surface properties of the templates including the chemistry, porosity and roughness can significantly impact heterogeneous crystal nucleation.[20,21] Oftentimes the influence of template surface properties on crystallisation has been studied at a specific temperature and solute concentration. However, from a process development perspective, it is important to determine the effect of template surfaces on the crystallisation phase diagram so as to enable identification of the operating regions for selective crystallisation of polymorphs.

In our previous communication,[22] we reported the effect of template chemistry on the nucleation of carbamazepine (CBZ) polymorphs at 20 °C in the supersaturation range 2.2–3.2 (corresponding to solute concentration 45–65 mg/ml). CBZ has four anhydrous polymorphs represented as triclinic form I, triagonal form II, *P*-monoclinic form III and *C*-monoclinic form IV.[23] A new polymorph, form V, of CBZ has been reported to form on the crystal facet of an analogous molecule, directed by epitaxial relationship.[11] The results from our previous study highlighted that template chemistry influenced the nucleation of CBZ polymorphs within a definite supersaturation range. Herein, we further explore the impact of templates with different chemistries on CBZ crystallisation by establishing template-induced polymorphic domain (TiPoD) plots as a function of crystallisation temperature (15–25 °C) and solute concentration (40-65 mg/ml). Solubility of form II and form III polymorphs in ethanol were measured so as to ascertain the difference in supersaturation driving force for nucleation of the two forms. Towards gaining a deeper understanding of the experimental observations, molecular modelling was performed to evaluate the interaction energies between the template surfaces and the two CBZ crystal polymorphs.

Methodology

Materials

Carbamazepine (5H-dibenzazepine-5-carboxamide), 3-cyanopropyl triethoxy silane (cyano silane), 3-mercaptopropyl trimethoxy silane (mercapto silane) and 3-trifluoropropyl trimethoxy silane (fluoro silane) (Figure 1) were purchased from Sigma Aldrich and used as received. AnalR NORMAPUR® ethanol (VWR) was used to prepare CBZ solutions. Toluene (VWR) was used for predissolving the organosilanes used for silanising the glass vials.

Silanisation and Template surface characterisation

Silanisation is a simple and common method used to chemically modify surfaces with different functional groups. 4 ml soda glass vials (diameter 12 mm and height 50 mm) were silanised using the method described in our previous paper.[22] Glass cover slips were silanised using the same procedure and subsequently analysed by contact angle measurements, X-ray photoelectron spectroscopy (XPS) and ellipsometry. The experimental procedures and data analysis are provided in the supplementary information.

Figure 1. Molecular structures of (a) Carbamazepine, (b)-(d) cyano, fluoro, and mercapto silanes, respectively.

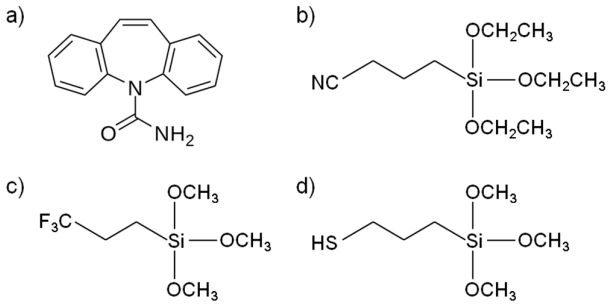

Crystallisation

Cooling crystallisation of CBZ under quiescent condition was conducted in silanised glass vials placed inside a temperature controlled incubator. Initial supersaturations (c/c*), ranging from 1.6–3.8, were generated by dissolving the required amount of solute in ethanol at an elevated temperature followed by a single step natural cooling to the different crystallisation temperatures (15, 20 and 25°C respectively). 3 ml of CBZ solution was added into the glass vial through 0.22 µm syringe filter to avoid any particulates or dust. The solution vials were then hermetically sealed to avoid evaporation of ethanol. Appearance of CBZ crystals in the vials was monitored using a digital USB optical microscope (VMS-004D, Veho, UK). For each template chemistry, at least 5 repeats of the experiments were carried out at each crystallisation temperature and supersaturation level. Control experiments were performed in clean glass vials at the same solution conditions.

Powder X-ray diffraction (XRD) analysis of the CBZ crystals was performed with an X'Pert PRO diffractometer (PANalytical, Almelo, The Netherlands) with nickel-filtered Cu Kα radiation operated at 40 kV and 40 mA. The samples were scanned in the range 3–60 ° 2θ using a step size of 0.01 ° with a count time of 2.5 seconds per step.

Solubility measurement

Solubility of form II and form III CBZ crystals in ethanol was measured using the Crystalline system (Avantium, The Netherlands). The apparatus works on the principle of 'clear point' measurement, the temperature at which a suspension with a known concentration of solid turns into a clear solution upon heating. In the case of stable form III polymorph, the clear point temperatures of a slurry suspension of CBZ (5 ml) were determined at four different heating rates (1, 0.5, 0.25 and 0.1 °C/min, respectively). By extrapolating the clear point data to "zero heating rate", the equilibrium dissolution temperature that is independent of the heating rate was determined. Solubility of form II CBZ was determined using an adapted bracketing method. In this method, multiple vials with solution samples saturated with a known quantity of the stable crystal form were first prepared and held at 0.25 °C (± 0.1 °C)

temperature intervals. 5 mg of form II crystals was added to each of the equilibrated solutions. If the initial solution concentration was below the solubility of the metastable form at that particular temperature, the added crystals fully dissolved (typically within 2–3 minutes). On the other hand, if the solution concentration was above the solubility limit, the added crystals did not dissolve fully and the excess solid underwent solution mediated transformation to the stable form over a period of time. Among the multiple solution samples, the lowest temperature at which the added form II crystals completely dissolved corresponded to the saturation temperature with respect to the metastable form.

Crystal face indexing

Data for crystal face indexing was collected using Agilent Xcalibur 3E (Agilent Technologies, Oxford, UK) diffractometer at room temperature. The crystal facets were indexed with the data analysed using CrysAlisPro (Agilent Technologies, Oxford, UK) software system.

Molecular modelling

The crystal habits of form II and form III CBZ polymorphs were simulated from their crystal structures using the BFDH (Bravais–Friedel–Donnay–Harker) and attachment energy (AE) models implemented in the *Morphology* module in Materials Studio (Accerlys Software Inc., USA, Version 5.5). While the BFDH model is based on crystallographic and geometric considerations, the AE model relates the energies of the bonds between the crystal-building units to its external shape.[24] Crystal structures of form II and form III polymorphs of CBZ were obtained from the Cambridge Crystallographic Data Centre (ref. codes CBMZPN03 and CBMZPN10, respectively).

The *Forcite* module in Materials Studio was used to simulate interactions between a silane monolayer and the (*hkl*) facets of CBZ crystal polymorphs. A silane monolayer comprised of 10 × 6 matrix of silane molecules substituted on the Si atom sites on a silica (100) face. The Si atoms of the silane monolayer were constrained in all three planes so as to maintain the monolayer pattern during molecular dynamics (MD) simulation. This assumption is valid since the Si atoms in silane molecule are attached to the glass substrate through covalent bonds. The morphologically important facets were cleaved from the CBZ crystal structure and a molecular cluster was built with a minimum dimension of 25 Å × 25 Å in X and Y axis and a thickness of 4 unit cells in the Z axis. The molecular cluster was constrained as a motion group, in which the coordinates of each molecule in the group remain fixed relative to the coordinates of all the other molecules in the group. However, the motion group as a whole can be translated or rotated along its centre of mass during geometry optimisation simulations, with the symmetry structure of the molecules being preserved. Defining the motion groups helps in optimising the facet orientation on a silane layer without losing the spatial arrangement of CBZ molecules within the cluster. The motion group was then positioned over the silane layer and *Quench* simulations were performed, which involved MD simulations followed by geometry optimisation. MD simulation was performed with COMPASS forcefield using NVT ensemble at 293 K for 1 ps with a time step of 1 fs. Geometry optimisation of the crystal facet cluster–silane monolayer system was performed at every 100 steps of dynamics using a smart algorithm implemented in Forcite. In this way, different initial configurations of the facet orientation on a silane monolayer template were sampled. After the Quench simulations, interaction energy between the silane monolayer and a crystal cluster was calculated using the relation:

Interaction energy = Total energy of the system – (Energy of the silane monolayer + Energy of the crystal cluster)

Likewise, interaction energy on the control surface is computed by substituting the silane monolayer with hydroxyl functional groups. Values of interaction energies calculated from these simulation trials were in turn used to interpret specific interactions between the silane monolayer and crystal polymorph. The implicit assumption underlying these molecular simulations is that prenucleation solute aggregates formed in supersaturated solution exhibit a certain degree of structural similarity to the mature crystal polymorph.[25,26, 27] Also, the effect of solvation on the interactions between the crystal facet and template surface is assumed to be relatively similar in the case of control and functionalised surfaces. Hence, the simulation does not incorporate solvents in the interaction energy calculations.

Results and Discussion

Characterisation of the Template Surfaces

The elemental composition on different templates calculated using XPS confirmed surface functionalisation (Table 1). Besides, XPS analysis on mercapto functionalised template revealed that about a third of the mercapto groups had formed di-sulphide bonds through cross linking on the surface. Through ellipsometry, the thickness of silane layer on the template surface was found to be 1.37 ± 0.03 nm, suggesting 2–3 layers of silane molecules. Surface energy values calculated from contact angle measurements showed that cyano functionalised template had a higher surface energy than mercapto and fluoro surfaces, respectively. It also revealed that the mercapto and fluoro surfaces had a low polar component of free energy.[22] Further details on surface characterisation are provided in the electronic supplementary information.

Table 1. Elemental concentrations on functionalised template surfaces in atomic percentages calculated from high resolution XPS spectra.

	C (%)	O (%)	Si (%)	N (%)	S (%)	F (%)
Cyano	45	35.4	16.3	3.3	-	-
Mercapto	54.3	30.1	10.2	-	5.4	-
Fluoro	31.3	38.1	17.9	-	-	12.7

Solubility of CBZ crystal polymorphs

The solubility curves of forms II (metastable) and III (stable) CBZ polymorphs in ethanol are shown in figure 2. Form III

solubility measured in this work shows good agreement with previously reported data.[28] In the temperature range from 10 to 30 °C, form II solubility is higher than form III solubility with a trend supporting a monotropic relationship between the two polymorphs.[23] The average solubility ratio of form II and form III in this temperature range is found to be 1.1. At 20 °C, this translates to 232 J/mol higher supersaturation driving force for nucleation of the stable form. In the ensuing sections, the supersaturation values are reported based on form III solubility.

Figure 2. Solubility of CBZ form II and form III in ethanol measured as a function of temperature. Form III literature values in mg/ml are calculated based on published data.[28]

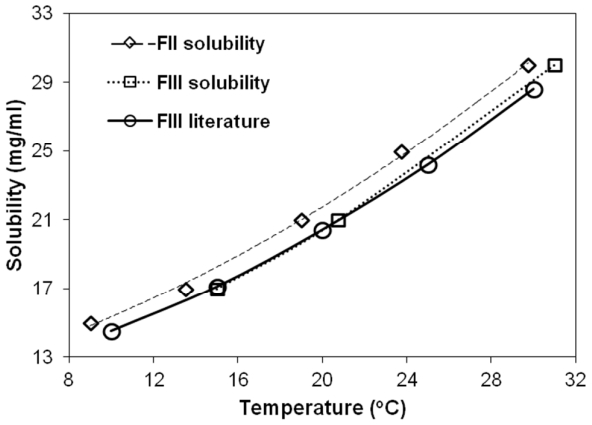

Template-induced Polymorphic Crystallisation

The polymorphic outcome for template-induced crystallisation of CBZ from ethanol solutions at various temperature and solute concentrations are represented with the help of a template-induced polymorphic domain (TiPoD) plot as shown in Figure 3. On the control surface, at any particular temperature, as the initial supersaturation is increased, the kinetically stable form II nucleates preferentially over form III. At lower supersaturations, nucleation of the thermodynamically stable form III crystals is dominant. At an intermediate range of supersaturation, concomitant nucleation of both polymorphic forms occurs. These observations are in-line with the reported behaviour for nucleation of CBZ polymorphs.[29,30] As seen from the TiPoD plot, supersolubility regions in which the stable and metastable polymorphs crystallised were altered upon using the template substrates. At 15 °C, concomitant nucleation of form II and form III CBZ occurred in control vials in the initial concentration range from 45 to 50 mg/ml (supersaturation range of 2.6–2.9). In contrast, at the same solute concentration and temperature, mercapto and fluoro surfaces predominantly nucleated form III CBZ while cyano functionalised surfaces nucleated form II crystals. At 20 °C and 25 °C respectively, crystallisation from solutions with initial concentrations in the range of 50–60 mg/ml (supersaturation range of 2.1 to 2.6 at 20 °C and 1.8 to 2.2 at 25 °C) resulted in concomitant nucleation of form II and form III polymorphs on the control surface. Under these solution conditions, templates with mercapto and fluoro functional groups led to preferential nucleation of form III crystals while cyano functionalised surfaces favoured nucleation of form II crystals. The effect of templates on polymorph selection was significant within a supersaturation range of 2.0 to 3.2, slightly beyond the regime where concomitant nucleation was observed. Outside this supersaturation range, little impact was observed on the nucleation behaviour with varying surface chemistry. Thus, the effect of template surface on crystal nucleation was significant within a restrained set of solution conditions.

In Figure 3, the polymorphic occurrence domains were extrapolated slightly beyond the temperature range at which the experimental observations were made so as to coincide with the solubility curves of the polymorphs. This extrapolation was done based on the observed trend in the polymorphic outcomes — for a given solute concentration, the stable polymorph (form III) crystallised preferentially at the

Figure 3. A schematic representation of template-induced polymorphic domains (TiPoD) for form II and form III CBZ crystallisation. The continuous and broken curves denote solubility of form III and form II polymorphs, respectively. Square symbols represent experimental conditions where only form II crystals were observed initially; star symbols represent concomitant nucleation of form II and form III, and circles denote form III nucleation. The shaded region only serves as a guide to highlight the domains where different observations were recorded and the domains are extrapolated beyond the experimental temperature range to emphasize the trend.

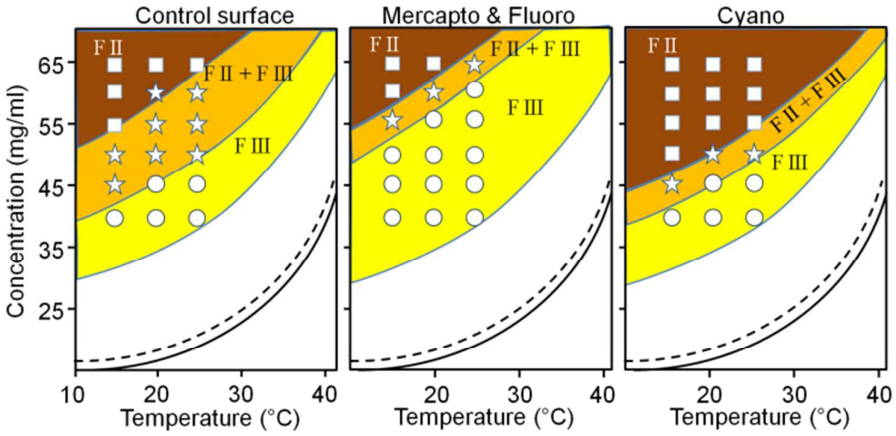

higher temperature on different template surfaces. The resulting TiPoD plots can be useful towards anticipating the polymorphic composition of a crystallisation experiment carried out at a particular solution condition and under the influence of specific surface chemistry. A future application of this concept would be to operate a crystallisation process within a specific region in the TiPoD plot by implementing process analytical technology (PAT) tools, which, in turn will aid in ensuring the product quality (polymorphic purity) through a Quality-by-Design approach.

At 15 °C, pure form II crystals nucleated on the control surface at concentrations above 55 mg/ml; while on the cyano surface, pure form II crystals nucleated at 50 mg/ml. Assuming that the mole fraction ratios correspond to the activity ratios of the solute in solution,[31] the free energy difference (ΔG) between the two crystallisation conditions (c – control substrate; t – template) can be calculated using the relationship,

$$\Delta G_T^{c,t} = -R\,T\ln(\frac{S_T^c}{S_T^t})$$

where R is the gas constant, T is the temperature, S^c and S^t are the solution concentrations (in mol fraction) at which pure crystal forms nucleated in the control and template vials. Using the above relationship and based on the minimum concentration value that resulted in form II crystallisation at the three different temperatures, an average free energy advantage of 344 ± 103 J/mol was calculated for form II nucleation on the cyano template over the control surface. Similarly, based on the maximum concentration at which pure form III crystallisation was obtained on the control, mercapto, and fluoro surfaces respectively, an average free energy advantage of 571 ± 116 J/mol was calculated for the nucleation of form III on mercapto and fluoro surfaces respectively, over the control surface. These energy values are comparable with the driving force contributions due to solubility differences between the two polymorphs, and are in line with shorter induction times for nucleation of CBZ crystals observed under the influence of different template surface chemistries.[22] Also, the free energy advantages gained in the presence of a template surface are in the order of very weak hydrogen bond and dispersive intermolecular interactions.[32] However, it has to be taken into consideration that these free energy differences are calculated based on the observed crystallisation outcome and hence need not directly translate to the kinetics and/or thermodynamics of the nucleation process. Also, the energy values are calculated solely based on the concentrations used in the experiments and the boundaries of the domains are subjective and dependent on other factors such as the cooling rate of crystallisation.

Probing Preferred Orientation Effects

Even as the polymorphic form nucleated on the template surfaces was confirmed from PXRD pattern of the harvested CBZ crystals, any preferred orientation effects of the crystals grown on the template surfaces were further examined. A typical XRD pattern of the as-grown crystals can exhibit high intensity diffraction peaks corresponding to dominant crystal planes parallel to the template surface.[33] To verify this, XRD pattern of form II and form III as-grown crystals were obtained while adhering to the template surface and, in turn, compared with the powder pattern of the harvested crystals (Figure 4). Form III CBZ crystallised on mercapto and fluoro templates exhibited strong peaks at 15.7° and 15.2° 2θ, corresponding to (010) and $(11\bar{1})$ planes respectively. It should also be noted that the XRD pattern of crystals from mercapto and fluoro templates exhibits small peaks at 8.7°, corresponding to form II polymorph. Hence, it could be concluded that the crystals obtained from these templates contain a mixture of form II and form III crystals with the latter forming the majority of the phase. On the cyano surface, form II needles were observed growing perpendicular to the template surface (Figure 5). Hence, diffraction peaks corresponding to the facets perpendicular to fast growing c-axis of the crystal were expected for inferring oriented growth of form II. However, form II CBZ crystals grown on cyano template exhibited strong peaks at 8.7° and 12.1° 2θ, corresponding to (100) and $(2\bar{1}0)$ facets parallel to the c-axis. This discrepancy could be reasoned as follows: upon removal of form II crystals from the crystallising solution, they tend to stick together in residual solution, fall over and lie parallel to the template surface. Since the preferred orientation effect caused due to acicular morphology of form II crystals is prominent, any preferred orientation effects due to the template-induced crystallisation of form II could not be confirmed.

Simulating Template-Crystal Facet Interaction Energy

While a de-novo simulation of primary crystal nucleation on a template surface using molecular dynamics is beyond the scope of this study, herein, we attempt to probe interaction energies between a pre-formed crystal cluster and a well-defined template surface. It is well recognised in the literature[26,27] that pre-nucleation aggregates are formed in a supersaturated solution and polymorphic structures compete to form a stable crystal nucleus as influenced by the solution conditions. Building on this premise, the ability of a template surface to induce heterogeneous nucleation of a specific polymorph is assessed by calculating the interaction energies of both form II and form II CBZ polymorphs (that are experimentally obtained from the control surface) with the template surfaces, as the polymorphic clusters approach the surface along different crystallographic orientations. It is postulated that favourable interaction energy between a crystal facet and template surface will assist heterogeneous nucleation of the crystal polymorph.

Initially, face indexing of form III CBZ crystal was performed to establish the morphologically relevant facets (Figure 6). Growth morphology of form II and form III polymorphs predicted using BFDH and attachment energy models exhibited similar results (Figure 7). While the predicted morphology of form II crystal is similar to the needle-shaped crystals obtained experimentally, the predicted morphology of

form III crystal differed significantly from the experimental crystal habit (cf. Figure 6). Form III predicted morphology exhibits several facets which were not observed during face indexing. This difference could be attributed to the influence of solvents on crystal habit, which are not incorporated in these morphology prediction methods.[34]

Figure 4.a) Powder X-ray diffractograms of form II and form III CBZ polymorphs crystallised from silanised vials and as-grown on glass cover slips; b) PXRD patterns CBZ polymorphs simulated from their crystal structures in Materials Studio Reflex module.

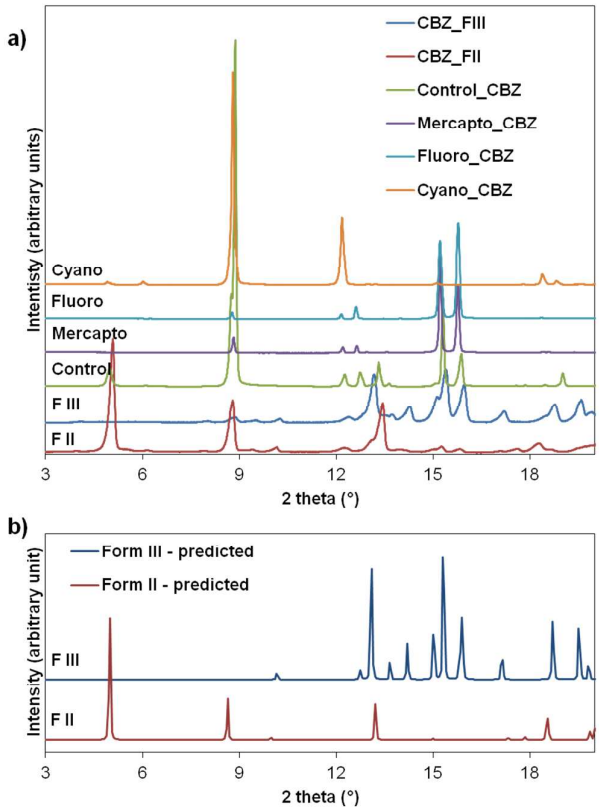

Figure 5. Form II needles growing perpendicular to the cyano template surface.

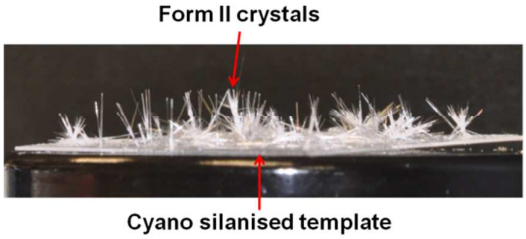

Figure 6. Indexed facets of form III CBZ crystal.

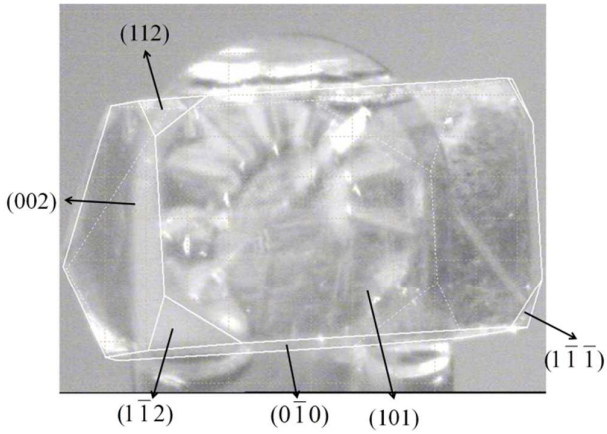

A snapshot of the cluster of CBZ molecules (modelled as a motion group) oriented on the template surface is depicted in Figure 8. The interaction energy between prominent facets of both form II and form III crystals and template surfaces are computed from the MD simulations and provided in Figure 9. A negative value for the interaction energy relates to favourable template-crystal cluster interaction, with the strength of intermolecular interactions being proportional to absolute value of the energy. Conversely, a positive value of interaction energy corresponds to unfavourable interaction between the crystal cluster and template. Interpreting the calculated interaction energy values on this basis, from Figure 9(b), the mercapto and fluoro functionalised surfaces show significant favourable interactions with (010) and $(\bar{1}11)$ facets of form III crystal. At the same time, both these templates exhibit highly positive (unfavourable) or mildly negative (favourable) interactions with form II dominant facet clusters (Figure 9(a)). In contrast, cyano functionalised template exhibits strong favourable interaction with form II clusters (cf. Figure 9a) along with significantly unfavourable interaction with (101) and $(1\bar{1}2)$ facets of form III (cf. Figure 9b). In comparison, the control (hydroxyl) surface exhibits somewhat favourable interaction with form II clusters and highly favourable interaction with (010) and $(\bar{1}11)$ facets of form III. Note that the focus here is on the relative values of interaction energy rather than the absolute values.

Figure 7. Predicted morphology of CBZ a) form II and b) form III polymorphs using i) attachment energy and ii) BFDH models.

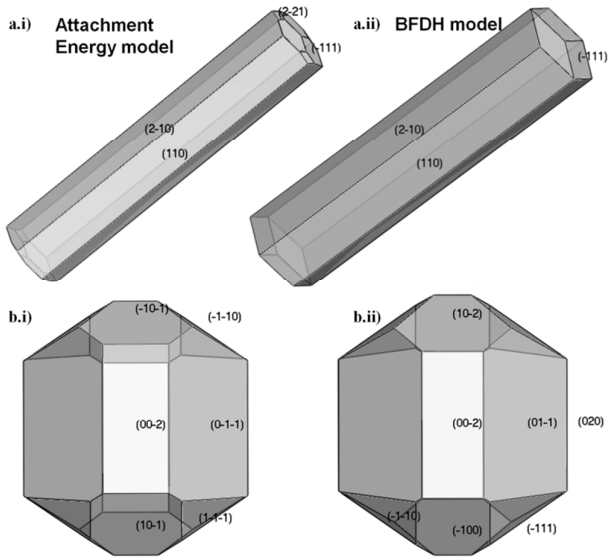

By analysing the interaction energy values of crystal clusters on each template surface, it can be inferred that the control surface has favourable interactions with both form II and form III crystals. On the other hand, mercapto and fluoro functionalised surfaces does not show significant interaction with form II while exhibiting strong favourable interactions with form III facets. The combined effects of these subtle intermolecular interactions could lead to predominant nucleation of form III crystals on mercapto and fluoro surfaces, respectively. Similarly, the synergistic effects of favourable and unfavourable interaction of cyano functionalised template towards form II and form III facets respectively can induce selective nucleation of form II crystals.

Figure 8. Motion group extracted from $(2\bar{2}1)$ facet of form II CBZ crystal oriented on mercapto silane template surface. Inset: top view of the molecular arrangement as observed along the b-axis.

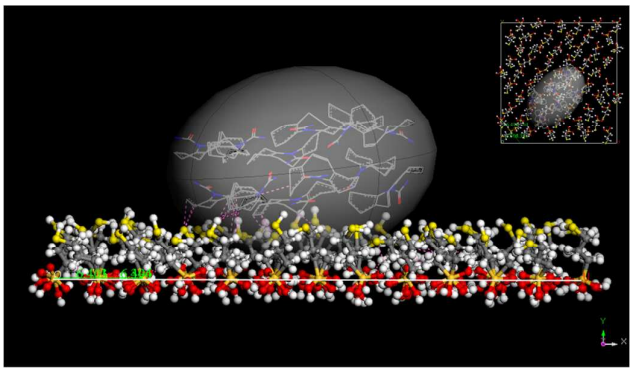

Further Discussion

Previous studies[35,36] have shown that the polymorphic outcome in CBZ crystallisation is dependent on the hydrogen bonding nature of the solvent. Solvents with a propensity to accept hydrogen bonds favoured form II nucleation, whereas solvents that are hydrogen bond acceptors and donors led to concomitant crystallisation of form II and form III. Evaluating the crystal structures of the two polymorphs, together with nucleation and polymorphic transformation kinetics data, Kelley and Rodriguez-Hornedo[35] proposed that specific interactions between solvent and CBZ molecules influenced self-association of CBZ molecules preceding crystal nucleation. Since CH···O interactions are critical in stabilizing the form III crystal structure, a solvent that primarily accepts hydrogen bonds can prevent the formation of molecular motif that is necessary for form III nucleation. On the other hand, since the CH···O interaction is not critical in stabilizing the form II crystal structure, its nucleation will be unaffected. In a subsequent study, Hunter et al.[36] investigated aggregation of CBZ molecules in solutions using NMR spectroscopy and found that dimerisation of CBZ molecules in polar solvents is mediated through aromatic interactions, whereas non-polar solvents facilitate dimerisation through hydrogen bonding between CBZ molecules. The dimer motifs formed under the influence of

Figure 9. Interaction energy of (a) form II CBZ facets and (b) form III CBZ facets with template surfaces calculated using molecular modelling

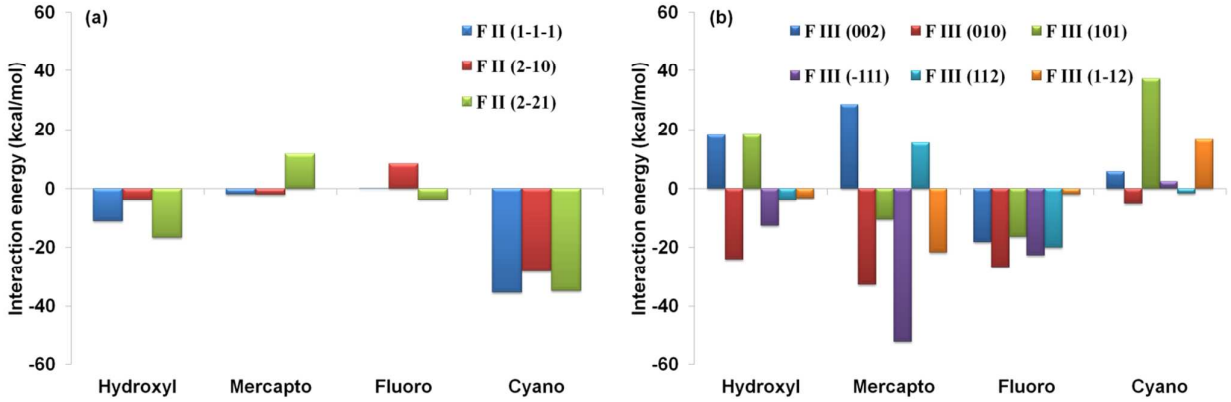

different solvent environment are preserved in the crystal polymorphs formed from the respective solvents.

By drawing analogy to the solvent effects on preferential nucleation of CBZ polymorphs, we envisage the role of functional groups on template-induced nucleation of specific CBZ crystal polymorphs. From a structural chemistry perspective, among the functionalised templates investigated in this study, the mercapto (–SH) head group can act as both acceptor and donor of hydrogen bond. On the other hand, both cyano (–CN) and fluoro ($–CF_3$) head groups can act as weak hydrogen bond acceptors. However, the results obtained from surface characterisation of the templates reveal that the cyano surface exhibited a much higher value of surface energy compared to the fluoro surface (see ESI Table S2). Moreover, the polar component of surface energy (arising from the basic component) for the cyano surface was determined to be significantly higher. These results indicate that the cyano template could act as a much stronger hydrogen bond acceptor and therefore — akin to a hydrogen bond acceptor solvent — promote nucleation of form II CBZ. Even as we propose a molecular recognition perspective to explain the experimental observations, it is noted that the thermodynamics and kinetics of homogeneous versus heterogeneous crystal nucleation could be significantly different.

The molecular modelling results suggest that interaction energy between the template surface and different facets of a crystal polymorph vary significantly. This variation could be attributed to heterogeneous nature of crystal facets,[37,38] whereby differences in surface functional groups and molecular spacing influence intermolecular interactions at the template-nucleating crystal interface. Nevertheless an epitaxial relationship between the template and crystal facet is not anticipated due to the characteristics of the functionalised templates used in this study.[22,39] Retrospectively, differences in the dipole moments, hydrogen bonding potentials, and polarity of both the crystal facet and template surfaces could be attributed to the preferential nucleation of crystal polymorphs. As mentioned before, one or more of these aspects can be effective in altering the thermodynamic (free energy barrier for crystal nucleation) and kinetic factors (molecular self assembling) that affect nucleation and crystal growth.[40] Furthermore, as highlighted in the TiPoD diagram, the effect of template on crystal nucleation is significant within a restrained set of operating conditions. This observation holds significance in the context of a template-induced crystallisation process development based on a Quality-by-design (QbD) approach.

Conclusions

Heterogeneous nucleation of CBZ crystal polymorphs was shown to be influenced by the chemistry of the template surfaces. These effects were tracked by determining template-induced polymorphic domains (TiPoD) for crystallisation of form II and form III on a concentration–temperature phase diagram. The relative free energy advantage calculated for template-induced crystallisation of polymorphs indicated that cyano-functionalised templates promoted nucleation of metastable form II polymorph and, in contrast, mercapto and fluoro surfaces favoured nucleation of stable form III. Interfacial interactions between the polymorphic crystal structures and the template surfaces were simulated through molecular modelling. Templates exhibiting favourable interaction with the dominant facets of a specific crystal polymorph were observed to promote nucleation of that particular polymorph. This approach can potentially be utilised to extend the knowledge on template-induced nucleation process for the selection of seeds with suitable surface properties to control crystal polymorphism.

Acknowledgement

The authors acknowledge Dr. Andrew J P White, Chemical Crystallography Laboratory, Imperial College London for his help with crystal face indexing.

References

1 S. Aitipamula, P. S. Chow and R. B. H. Tan, *CrystEngComm*, 2014, **16**, 3451.
2 A. Y. Lee, D. Erdemir and A. S. Myerson, *Annu. Rev. Chem. Biomol. Eng.*, 2011, **2**, 259-280.
3 A. Llinas and J. M. Goodman, *Drug Discovery Today*, 2008, **13**, 198-210.
4 C. Sudha and K. Srinivasan, *CrystEngComm*, 2013, **15**, 1914.
5 W. Beckmann, K. Nickisch and U. Budde, *Org. Process Res. Dev.*, 1998, **2**, 298-304.
6 L. Yu, *J. Am. Chem. Soc.*, 2003, **125**, 6380-6381.
7 S. K. Poornachary, J. V. Parambil, P. S. Chow, R. B. H. Tan and J. Y. Y. Heng, *Cryst. Growth Des.*, 2013, **13**, 1180-1186.
8 P. Asanithi, *J. Biomed. Mater. Res., Part A*, 2014, **102**, 2590-2599.
9 C. Capacci-Daniel, K. J. Gaskell and J. A. Swift, *Cryst. Growth Des.*, 2010, **10**, 952-962.
10 J.-M. Ha, B. D. Hamilton, M. A. Hillmyer and M. D. Ward, *Cryst. Growth Des.*, 2009, **9**, 4766-4777.
11 J.-B. Arlin, L. S. Price, S. L. Price and A. J. Florence, *Chem. Commun.*, 2011, **47**, 7074-7076.
12 A. Caridi, S. A. Kulkarni, G. Di Profio, E. Curcio and J. H. ter Horst, *Cryst. Growth Des.*, 2014, **14**, 1135-1141.
13 J. Zhang, A. Liu, Y. Han, Y. Ren, J. Gong, W. Li and J. Wang, *Cryst. Growth Des.*, 2011, **11**, 5498-5506.
14 A. Kwokal, T. T. H. Nguyen and K. J. Roberts, *Cryst. Growth Des.*, 2009, **9**, 4324-4334.
15 A. I. Toldy, L. Zheng, A. Z. M. Badruddoza, T. A. Hatton and S. A. Khan, *Cryst. Growth Des.*, 2014, **14**, 3485-3492.
16 U. V. Shah, D. R. Williams and J. Y. Y. Heng, *Cryst. Growth Des.*, 2012, **12**, 1362-1369.
17 C. Sudha, R. Nandhini and K. Srinivasan, *Cryst. Growth Des.*, 2014, **14**, 705-715.
18 V. Lopez-Mejias, J. W. Kampf and A. J. Matzger, *J. Am. Chem. Soc.*, 2009, **131**, 4554-4555.
19 Y. Diao, K. E. Whaley, M. E. Helgeson, M. A. Woldeyes, P. S. Doyle, A. S. Myerson, T. A. Hatton and B. L. Trout, *J. Am. Chem. Soc.*, 2011, **134**, 673-684.

20 K. Chadwick, A. Myerson and B. Trout, *CrystEngComm*, 2011, **13**, 6625.

21 Y. Diao, A. S. Myerson, T. A. Hatton and B. L. Trout, *Langmuir*, 2011, **27**, 5324-5334.

22 J. V. Parambil, S. K. Poornachary, R. B. H. Tan and J. Y. Y. Heng, *CrystEngComm*, 2014, **16**, 4927.

23 A. L. Grzesiak, M. Lang, K. Kim and A. J. Matzger, *J. Pharm. Sci.*, 2003, **92**, 2260-2271.

24 S. K. Poornachary, P. S. Chow and R. B. H. Tan, in *Molecular Modeling for the Design of Novel Performance Chemicals and Materials*, CRC Press, 2012, DOI: doi:10.1201/b11590-6, pp. 157-185.

25 A. Mattei and T. Li, *Pharm. Res.*, 2011, **29**, 460-470.

26 R. J. Davey, N. Blagden, S. Righini, H. Alison, M. J. Quayle and S. Fuller, *Cryst. Growth Des.*, 2001, **1**, 59-65.

27 R. A. Sullivan, R. J. Davey, G. Sadiq, G. Dent, K. R. Back, J. H. ter Horst, D. Toroz and R. B. Hammond, *Cryst. Growth Des.*, 2014, **14**, 2689-2696.

28 M. A. O'Mahony, D. M. Croker, Å. C. Rasmuson, S. Veesler and B. K. Hodnett, *Org. Process Res. Dev.*, 2013, **17**, 512-518.

29 S. Teychené and B. Biscans, *Cryst. Growth Des.*, 2008, **8**, 1133-1139.

30 A. J. Florence, A. Johnston, S. L. Price, H. Nowell, A. R. Kennedy and N. Shankland, *J. Pharm. Sci.*, 2006, **95**, 1918-1930.

31 G. S. Parks, L. J. Snyder and F. R. Cattoir, *J. Chem. Phys.*, 1934, **2**, 595.

32 G. R. Desiraju, *Angew. Chem., Int. Ed.*, 2011, **50**, 52-59.

33 J. H. Urbelis and J. A. Swift, *Cryst. Growth Des.*, 2014, **14**, 5244-5251.

34 D. Winn and M. F. Doherty, *AIChE J.*, 2000, **46**, 1348-1367.

35 R. C. Kelly and N. Rodríguez-Hornedo, *Org. Process Res. Dev.*, 2009, **13**, 1291-1300.

36 C. A. Hunter, J. F. McCabe and A. Spitaleri, *CrystEngComm*, 2012, **14**, 7115.

37 R. Ho, D. A. Wilson and J. Y. Y. Heng, *Cryst. Growth Des.*, 2009, **9**, 4907-4911.

38 S. R. Modi, A. K. R. Dantuluri, S. R. Perumalla, C. C. Sun and A. K. Bansal, *Cryst. Growth Des.*, 2014, **14**, 5283-5292.

39 D. Lee, G. Monin, N. T. Duong, I. Z. Lopez, M. Bardet, V. Mareau, L. Gonon and G. De Paepe, *J Am Chem Soc*, 2014, **136**, 13781-13788.

40 E. Curcio, V. López-Mejías, G. Di Profio, E. Fontananova, E. Drioli, B. L. Trout and A. S. Myerson, *Cryst. Growth Des.*, 2014, **14**, 678-686.

Graphical Abstract